

# The scaling relation between richness and mass of galaxy clusters: a Bayesian approach

S. Andreon<sup>1★</sup> and M. A. Hurn<sup>2</sup>

<sup>1</sup>*INAF–Osservatorio Astronomico di Brera, Milano, Italy*

<sup>2</sup>*Department of Mathematical Sciences, University of Bath, Bath*

Accepted 2010 January 22. Received 2010 January 11; in original form 2009 April 27

## ABSTRACT

We use a sample of 53 galaxy clusters at  $0.03 < z < 0.1$  with available masses derived from the caustic technique and with velocity dispersions computed using 208 galaxies on average per cluster, in order to investigate the scaling between richness, mass and velocity dispersion. A tight scaling between richness and mass is found, with an intrinsic scatter of only 0.19 dex in mass and with a slope one, i.e. clusters that have twice as many galaxies are twice as massive. When richness is measured without any knowledge of the cluster mass or linked parameters (such as  $r_{200}$ ), it can predict mass with an uncertainty of  $0.29 \pm 0.01$  dex. As a mass proxy, richness competes favourably with both direct measurements of mass given by the caustic method, which has typically 0.14 dex errors (versus 0.29) and X-ray luminosity, which offers a similar 0.30 dex uncertainty. The similar performances of X-ray luminosity and richness in predicting cluster masses has been confirmed using cluster masses derived from velocity dispersion fixed by numerical simulations. These results suggest that cluster masses can be reliably estimated from simple galaxy counts, at least at the redshift and masses explored in this work. This has important applications in the estimation of cosmological parameters from optical cluster surveys, because in current surveys clusters detected in the optical range outnumber, by at least one order of magnitude, those detected in X-ray. Our analysis is robust from an astrophysical perspective because the adopted masses are among the most hypothesis-parsimonious estimates of cluster mass and from a statistical perspective, because our Bayesian analysis accounts for terms usually neglected, such as the Poisson nature of galaxy counts, the intrinsic scatter and uncertain errors. The data and code used for the stochastic computation are provided in the paper.

**Key words:** methods: statistical – galaxies: clusters: general – galaxies: elliptical and lenticular, cD – galaxies: luminosity function, mass function – cosmological parameters – X-rays: galaxies: clusters.

## 1 INTRODUCTION

Clusters of galaxies are attracting considerable attention for their cosmological applications. A conceptually simple observation, such as the number of clusters per unit volume, is able to put strong constraints on the cosmological parameters (or their combinations); for example, on the equation of state of the dark energy (e.g. Albrecht et al. 2006; i.e. the Dark Energy Report, and references therein). In essence, both analytic predictions and gravitational N body simulations give the halo mass function,  $dN/dM/dV$ , i.e. the number of halos of mass  $M$  per unit halo mass and universe volume. The number of halos is sensitive to the cosmological parameters in two ways:

linearly (with the cosmic volume) and exponentially (via the growth function, i.e. how the cluster mass increases with time). Since one can in principle measure the abundance of the clusters in the Universe, the comparison of the observed number of clusters to the expected (cosmologically-dependent) number of halos allows one to constrain the cosmological parameters. This is one of the drivers of many on-going cluster surveys, such as the South Pole Telescope Survey<sup>1</sup> using clusters detected by the Sunyaev–Zel’dovich (SZ) effect, the XMM-Large Scale Survey,<sup>2</sup> the XMM-Cluster Survey<sup>3</sup> using clusters detected by their X-ray emission, MaxBCG (Koester

★E-mail: stefano.andreon@brera.inaf.it

<sup>1</sup> PI Carlstrom, <http://pole.uchicago.edu/>

<sup>2</sup> PI Pierre, <http://vela.astro.ulg.ac.be/themes/spatial/xmm/LSS/>

<sup>3</sup> PI Romer, <http://xcs-home.org/>

et al. 2007a) and the Red Sequence Cluster Survey<sup>4</sup> using clusters detected by optical data. More recently, lensing cluster surveys have started (e.g. Bergé et al. 2008).

As is known, each experiment measures a combination of cosmological parameters, rather than the parameters *per se*. Only the combination of several measures from different kinds of experiments is able to break this degeneracy in the parameter space, also showing the absence of systematic effects. In this sense, cluster counting is complementary to other experiments such as the observations of SNIa, or the measurements of Baryon Acoustic Oscillations and CMB, etc. This last aspect is very important in order to test the idea that dark energy is indeed a new source in Einstein equations rather than e.g. the manifestation of a different theory of gravity; by comparing observables that are mainly sensitive to the growth of structures with tests of the redshift–distance relation, we can look for inconsistencies that cannot be explained by dark energy in the form of a new fluid (e.g. Trota & Bower 2006).

The main obstacle to using clusters for cosmological tests is that no technique is able to yield a direct measure of their masses, but instead they measure proxies such as the X-ray flux, temperature or  $Y_x$  (Kravtsov, Vikhlinin & Nagai 2006),  $n_{200}$  (a sort of galaxy richness; see below) or the SZ decrement.

The calibration between mass and mass proxy (average relation and intrinsic scatter) can be achieved either by specific follow-up observations (more direct, or at least independent, measures of mass), or by a Bayesian technique called in the astronomical context self-calibration (Majumdar & Mohr 2004; Gladders et al. 2007), i.e. basically modelling the relation with generic functions and marginalizing over their parameters. However, cosmological constraints are much less tight when determined in the absence of an external measure of the mass-scaling of the mass proxy. In particular, recent work by Wu, Rozo & Wechsler (2008) has emphasized how self-calibration is hampered by secondary parameters (i.e. the halo formation time and concentration). Therefore, a direct measurement of the scaling relation is essential to test the assumption of the self-calibration technique, namely to determine the shape of the scatter (currently Gaussian) and of the scaling (currently linear in log units) and this is a valuable aim *per se*.

The caustic method (Diaferio & Geller 1997; Diaferio 1999) offers a robust path to estimating cluster mass. It relies on the identification in projected phase-space (i.e. in the plane of line-of-sight velocities and projected cluster-centric radii,  $v$ ,  $R$ ) of the envelope defining sharp density contrasts (i.e. caustics) between the cluster and the field region. The amplitude of such an envelope is a measure of the mass inside  $R$ . Of course, there are other observables available for measuring cluster masses, but these require additional hypotheses. X-ray-determined masses require measurements of temperature and surface brightness profiles and are based on the assumption that the cluster hot gas is in hydrostatic equilibrium, an assumption that has been questioned in recent years (e.g. Rasia et al. 2006). Masses derived using SZ decrements additionally assume the intra-cluster medium is isothermal (e.g. Muchovej et al. 2007). In this paper, we use caustic masses, i.e. masses derived from the caustic technique that assumes that galaxies trace the velocity field. As opposed to the dynamical masses, derived from the virial theorem (i.e. from the velocity dispersion) or from the Jeans method, caustic mass does not require that the cluster is in dynamical equilibrium (see Rines & Diaferio 2006 for a discussion). On the other hand, the relative novelty of caustic masses make them much less studied through

numerical simulations and by comparisons to other mass proxies. For this reason, we look for systematic errors on caustic masses and we calibrate the mass–richness scaling with velocity dispersion and with an additional mass proxy based on velocity dispersion fixed by numerical simulations.

In this paper we aim to give the absolute calibration of the relation between  $n_{200}$ , the number of red galaxies (brighter than a specified limit and within a given cluster-centric distance) and mass. We also want to measure the scatter of the  $n_{200}$  mass proxy and compare its performance to the  $L_x$  mass proxy.

The mass–richness calibration was partially addressed in the pioneering work of maxBCG (Koester et al. 2007a; Rozo et al. 2007 and references therein). Because these works lack clusters with known masses and  $r_{200}$  and their analysis suffers from circularity ( $r_{200}$  is derived for stack of clusters of a given  $n_{200} = n(<r_{200})$ , i.e. of clusters with a known  $r_{200}$ ), their calibration is doubtful, and in fact, their  $r_{200}$ , used to measure  $n_{200}$ , is found in later papers to be on average twice as large as the assumed  $r_{200}$  radius (e.g. Becker et al. 2007; Johnston et al. 2007; Sheldon et al. 2009), i.e. they counted galaxies in a radius too large by a factor of two. Furthermore, they found a redshift dependence when none is assumed to be there by definition (Becker et al. 2007; Rykoff et al. 2008; Rozo et al. 2009). Our analysis does not share the problems they encountered.

Throughout this paper we assume  $\Omega_M = 0.3$ ,  $\Omega_\Lambda = 0.7$  and  $H_0 = 70 \text{ km s}^{-1} \text{ Mpc}^{-1}$ . In this paper, velocity dispersion, usually denoted by  $\sigma_v$  in the literature, is denoted with the symbol  $s$ . All quantities are measured in the usual units: velocity dispersions in  $\text{km s}^{-1}$ , cluster radii in kpc, X-ray luminosities in  $\text{erg s}^{-1}$ , cluster masses in solar mass units.

## 2 PARAMETER ESTIMATION IN BAYESIAN INFERENCE

The Bayesian approach to statistics has become increasingly popular over the past few decades as computational and algorithmic advances have permitted the analysis of more complex data sets and the use of more flexible models. For the theoretician, there are interesting philosophical differences to be explored between the Bayesian and frequentist approaches. For the practitioner, Bayesian data analysis provides an additional valuable statistics tool. A good introduction to the Bayesian framework can be found in many textbooks (e.g. D’Agostini 2003; MacKay 2003; Gelman et al. 2004). In this section we will summarize a Bayesian approach to an applied problem.

Suppose one is interested in estimating the (log) mass of a galaxy cluster,  $\lg M$ . In advance of collecting any data, we may have certain beliefs and expectations about the values of  $\lg M$ . In fact, these thoughts are often used in deciding which instrument will be used to gather data and how this instrument may be configured. For example, if we are wanting to measure the mass of a poor cluster via the virial theorem, a Jeans analysis or the caustic technique, we will select a spectroscopic set up with adequate resolution, in order to avoid that velocity errors are comparable to, or larger than, the likely low velocity dispersion of poor clusters. Crystallizing these thoughts in the form of a probability distribution for  $\lg M$  provides the prior  $p(\lg M)$ , used, as mentioned, in the feasibility section of the telescope time proposal, where instrument, configuration and exposure time are set.

For example, one may believe (e.g. from the cluster being somewhat poor) that the log of the cluster mass is probably not far from 13, plus or minus 1; this might be modelled by saying that the probability distribution of the log mass, here denoted by  $\lg M$ , is a

<sup>4</sup> PI Yee, <http://www.rcs2.org/>

Gaussian centred on 13 and with  $\sigma$ , the standard deviation, equal to 0.5, i.e.  $lgM \sim \mathcal{N}(13, 0.5^2)$ .

Once the appropriate instrument and its set up have been selected, data can be collected on the quantities of interest. In our example, this means we record a measurement of log mass, say  $obslgM200$ , via, for example, a caustic analysis, i.e. measuring distances and velocities. The physics or, sometimes simulations, of the measuring process may allow us to estimate the reliability of such measurements. Repeated measurements are also extremely useful for assessing it. The likelihood is the model that we adopt for how the noisy observation  $obslgM200$  arises given a value of  $lgM$ . For example, we may find that the measurement technique allows us to measure masses in an unbiased way but with a standard error of 0.1 and that the error structure is Gaussian, i.e.  $obslgM200 \sim \mathcal{N}(lgM, 0.1^2)$ . If we observe  $obslgM200 = 13.3$ , we usually summarize the above by writing  $lgM = 13.3 \pm 0.1$ .

How do we update our beliefs about the unobserved log mass  $lgM$  in light of the observed measurement,  $obslgM200$ ? Expressing this probabilistically, what is the posterior distribution of  $lgM$  given  $obslgM200$ , i.e.  $p(lgM|obslgM200)$ ? Bayes Theorem (Bayes 1764 and Laplace 1812) tells us that

$$p(lgM|obslgM200) = \frac{p(obslgM200|lgM)p(lgM)}{p(obslgM200)}. \quad (1)$$

The denominator  $p(obslgM200)$ , known as the (Bayesian) evidence, is equal to the integral of the numerator

$$p(obslgM200) = \int p(obslgM200|lgM)p(lgM)d lgM. \quad (2)$$

Notice that, as with frequentist statistical approaches, assumptions have been made that should be assessed; neither priors nor likelihoods (on which frequentist methods such as maximum likelihood estimation is based) are set in stone.

Simple algebra shows that in our example the posterior distribution of  $lgM|obslgM200$  is Gaussian, with mean  $\mu = \frac{13.0 \cdot 0.5^2 + 13.3 \cdot 0.1^2}{1/0.5^2 + 1/0.1^2} = 13.29$  and  $\sigma^2 = \frac{1}{1/0.5^2 + 1/0.1^2} = 0.0096$ .  $\mu$  is just the usual weighted average of two ‘input’ values, the prior and the observation, with weights given by prior and observation  $\sigma$ s.

In our example, the posterior mean and standard deviation are numerically almost indistinguishable from the observed value and its quoted error; however, this is not the rule for complex data analysis; for example, when biases are there or in frontier measurements, like in Butcher–Oemler studies, where one often finds observed values outside the range of acceptable values (see, e.g. Andreon et al. 2006a). From a computational point of view, only simple examples such as the one described above can generally be tackled analytically. Markov chain Monte Carlo (MCMC) methods are widely used for more complex problems.

Although this might sound intimidating to the astronomical end-user, the advent of BUGS-like programs (Spiegelhalter et al. 1996), such as JAGS (Plummer 2008), allow scientists to apply these ideas for quite complicated models using a simple syntax. In our example, we just need to write in an ASCII file the symbolic expression of the prior,  $lgM \sim \mathcal{N}(13, 0.5^2)$ , and likelihood,  $obslgM200 \sim \mathcal{N}(lgM, 0.1^2)$ , and nothing more. For the work in this paper, the JAGS code is given in Appendix B.

### 3 UNCERTAINTIES OF PREDICTED VALUES IN BAYESIAN INFERENCE

Suppose we want to estimate the value of a quantity not yet measured (e.g. the mass of a not-yet-weighted cluster). Before data  $lgM$  are

collected (or even considered), the distribution of the predicted values  $lg\tilde{M}$  can be expressed:

$$p(lg\tilde{M}) = \int p(lg\tilde{M}, \theta) d\theta = \int p(lg\tilde{M}|\theta)p(\theta) d\theta. \quad (3)$$

These two equalities result from the application of probability definitions, the first equality is simply that a marginal distribution results from integrating over a joint distribution, the second one is Bayes’ rule.

If some data  $lgM$  have already been collected for similar objects, we can use these data to improve our prediction for  $lg\tilde{M}$ . For example, if mass and richness in clusters are highly correlated, one may better predict the cluster mass knowing its richness than in the absence of such information, simply because mass shows a lower scatter at a given richness than when clusters of all richnesses are considered (except if the relationship has slope exactly equal to  $\tan k\pi/2$ , with  $k = 0, 1, 2, 3$ ). In making explicit the presence of such data,  $lgM$ , we rewrite equation (3) conditioning on  $lgM$ :

$$p(lg\tilde{M}|lgM) = \int p(lg\tilde{M}|lgM, \theta)p(\theta|lgM) d\theta. \quad (4)$$

The conditioning on  $lgM$  in the first term in the integral simplifies out because  $lgM$  and  $lg\tilde{M}$  are considered conditionally independent given  $\theta$ , so that this term becomes simply  $p(lg\tilde{M}|\theta)$ . The left-hand side of the equation is called the posterior predictive distribution for a new unobserved  $lg\tilde{M}$  given observed data  $lgM$  and model parameters  $\theta$ . Its width is a measure of the uncertainty of the predicted value  $lg\tilde{M}$ , a narrower distribution indicating a more precise prediction.

Let us first consider a simple example. Suppose we do not know the mass,  $lg\tilde{M}$ , of a given cluster and we are interested in predicting it from our knowledge of its richness. In this didactical example, we assume for simplicity that (a) all probability distributions are Gaussian, (b) that previous data  $lgM$  for clusters of the same richness allowed us to determine that clusters of that richness have on average a mass of  $lgM = 13.3 \pm 0.1$ , i.e.  $p(\theta|lgM) = \mathcal{N}(13.3, 0.1^2)$  and (c) that the scatter between the individual and the average mass of the clusters is 0.5 dex, i.e.  $p(lg\tilde{M}|\theta) = \mathcal{N}(\theta, 0.5^2)$ . Then, equation (4) is easily analytically solvable and gives the intuitive solution that  $p(lg\tilde{M}|lgM)$  is a Gaussian centred on  $lgM = 13.3$  and with a  $\sigma$  given by the sum in quadrature of 0.1 and 0.5 ( $=0.51$  dex). Therefore, a not-yet-weighted cluster of the considered richness has a predicted mass of 13.3 with an uncertainty of 0.51 dex. The latter is the performance of richness as a mass estimator in our didactical example. A different proxy, say X-ray luminosity, may give a different value for the uncertainty of the predicted mass and the comparison of these values allows us to rank the performances of these different mass proxies.

Later in this paper, we measure and compare the performance of mass and X-ray luminosity. The assumptions we use then go beyond the simplistic ones of the pedagogical example, starting with the assumption of having a set of clusters with richness identical to that of the cluster whose mass we want to estimate, the (tacit) assumption of living in an observational error-free world, the lack of modelling of a trend between richness and mass, the perfect knowledge of the parameters of the sampling distribution, a perfect matching of the richness of clusters with available mass and those with to-be-estimated mass, etc. Despite this apparent complexity, to account for all these factors, we only need to state a richness–mass scaling model (the same one used to analyse the scaling itself, detailed in Section 6.1) and use equation (4) to measure the performances of the mass proxies.

Although the above methodology might appear initially intimidating to the astronomical end-user, the use of predictive posterior distributions is generally pain free since programs such as BUGS offer it as a standard feature. In practice, the integral in equation (4) is computed quite simply using sampling; repeatedly values of  $\theta$  are drawn from the posterior  $p(\theta|l\tilde{g}M)$  and for each of these, values of  $\tilde{l\tilde{g}M}$  are drawn from  $p(\tilde{l\tilde{g}M}|\theta)$ . The values of  $\tilde{l\tilde{g}M}$  are stored. The width of the distribution of these values gives the uncertainty of the predicted value, i.e. the performance of the considered mass proxy. Therefore, the quoted performance accounts for all terms entering into the modelling of proxy and mass, which include the uncertainty of the proxy value (richness and X-ray luminosity), the uncertainty on the parameters describing the regression between mass and mass proxy (slope, intercept, intrinsic scatter and their covariance), as well as other modelled terms (we also account for the noisiness of the error itself in our analysis). Some factors are automatically accounted for without any additional input; for example, where data are scarce, for example near or outside the sampled richness or  $L_X$  range, predictions are noisier (because the regression is poorly determined here). As a consequence, proxy performances are poorer (the posterior predictive distribution is wider) there.

#### 4 PREDICTION WITH ERRORS ON PREDICTOR VARIABLES

It is important to distinguish between the prediction of a variable  $y$  which is assumed to be linearly related to a *non-random* predictor variable  $x$ , and the prediction of a variable  $y$  which is linearly related to a predictor variable  $x$  which is itself a random variable. The latter situation is the one in which we find ourselves here, given that we want to predict mass as a function of richness and for both quantities we must collect observational data.

Fig. 1 shows a set of 500 points drawn from a bivariate Gaussian where marginally both  $x$  and  $y$  are standard Gaussian with mean 0 and variance 1 and  $x$  and  $y$  have correlation 1/2. Superimposed on the left-hand panel of Fig. 1 is the line giving the theoretical conditional expectation of  $y$  given  $x$  (this is known theoretically for this bivariate Gaussian to be  $y = 0.5x$ ). By eye, this line perhaps seems too shallow with respect to the trend identified by the points, which perhaps might be captured by the  $x = y$  line shown in blue in the right-hand panel. However, if what we want to do is to predict a  $y$  given an  $x$  value, this ‘too shallow’ line is more appropriate. To illustrate why this is the case, the middle panel of Fig. 1 concentrates

on those observed for  $x$  close to 2. It is clear from their histogram that their average is closer to the value predicted by the red line (1 in this case) than the value predicted by the blue (2 in this case). To emphasize that although we treat  $x$  and  $y$  symmetrically in terms of both being random variables, we have an asymmetry in terms of our predictive goals, the right-hand panel also shows the expected value of  $x$  given a value of  $y$ .

Akritis & Bershad (1996) give a related description of the various types of fit from a non-Bayesian perspective.

#### 5 DATA & DATA REDUCTION

Our starting point is the CIRS (Cluster Infall Regions in SDSS, Rines & Diaferio 2006) cluster catalogue. Fundamentally, clusters are: (a) X-ray flux-selected, (b) with an upper cut at redshift  $z = 0.1$  (to allow a good caustic measurement) and (c) are in the SDSS DR6 spectroscopic survey. These catalogues give cluster centres, virial radii  $r_{200}$  and masses within  $r_{200}$ ,  $M_{200}$ , derived by the caustic technique. CIRS also lists the cluster velocity dispersion, computed using just those galaxies inside the caustic, and the turnaround radius. The velocity dispersions are computed using, on average, 208 member galaxies per cluster. We note that in CIRS velocity dispersions are quoted with slightly asymmetric errors. D’Agostini (2004) suggests adopting the average of the asymmetric errors as a point value of the error and the mid-point between the upper and lower values as a point value of the measurement (velocity dispersion) itself. Masses, as quoted by CIRS, have more asymmetric errors and are such that the lower error bar includes negative mass for some clusters. This is compatible with symmetric errors on a log scale being transformed on to a linear scale and is supported by the way in which Rines & Diaferio (2010) summarize in their introduction their previous (CIRS) paper. Therefore, we convert errors back on the log scale. Our statistical analysis accounts for noisiness of mass and velocity dispersion estimated errors.

For each cluster, we extract the galaxy catalogues from the Sloan Digital Sky Survey (hereafter SDSS) sixth data release (Adelman-McCarthy et al. 2008), discarding both clusters at  $z < 0.03$  to avoid shredding problems (large galaxies are split in many smaller sources) and two cluster pairs (requiring a deblending algorithm for estimating the richness of each cluster component). We also discard clusters not wholly enclosed inside the SDSS footprint and a few clusters with hierarchical centres that have converged on a secondary galaxy clump, instead of on the main cluster. One further cluster, the NGC4325 group, has been removed because it is

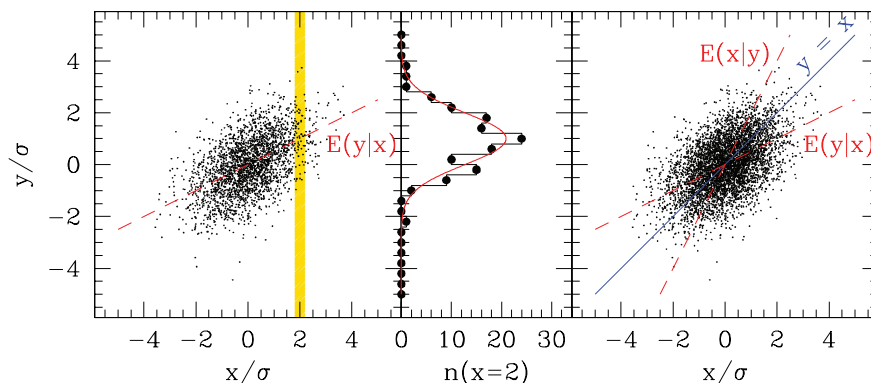


**Figure 1.** Left panel: 500 points drawn from a bivariate Gaussian, overlaid by the line showing the expected value of  $y$  given  $x$ . The yellow vertical stripe captures those  $y$  for which  $x$  is close to 2. Central panel: Distribution of the  $y$  values for  $x$  values in a narrow band of  $x$  centred on 2, as shaded in the left panel. Right panel: as the left panel, but we also add the lines joining the expected  $x$  values at a given  $y$ , and the  $x = y$  line.

**Table 1.** Observed galaxy counts and solid angle ratios. Columns 2 and 3 list the observed galaxy counts in the cluster and control directions. The latter subtend a solid angle  $C$  times larger than the former. Columns 5 and 6 repeat the content of Columns 2 and 4, but for a different cluster solid angle, whose radius is determined by equation (18), which uses the galaxy counts listed in Column 7.

| Cluster id<br>(1) | <i>obstot</i><br>(2) | <i>obsbkg</i><br>(3) | $C$<br>(4) | $\widehat{obstot}$<br>(5) | $\widehat{C}$<br>(6) | <i>obsn</i> ( $<1.43$ )<br>(7) |
|-------------------|----------------------|----------------------|------------|---------------------------|----------------------|--------------------------------|
| A0160             | 28                   | 13                   | 3.107      | 29                        | 2.951                | 31                             |
| A0602             | 45                   | 37                   | 3.186      | 23                        | 10.77                | 29                             |
| A0671             | 44                   | 20                   | 2.545      | 36                        | 5.443                | 37                             |
| A0779             | 27                   | 0                    | 0.2245     | 19                        | 0.4303               | 29                             |
| A0957             | 33                   | 20                   | 4.605      | 26                        | 7.947                | 29                             |
| A0954             | 27                   | 168                  | 44.87      | 28                        | 41.05                | 29                             |
| A0971             | 63                   | 127                  | 9.957      | 50                        | 19.57                | 47                             |
| RXCJ1022.0+3830   | 30                   | 28                   | 8.598      | 26                        | 10.27                | 33                             |
| A1066             | 76                   | 41                   | 4.075      | 65                        | 6.421                | 58                             |
| RXJ1053.7+5450    | 48                   | 70                   | 6.381      | 40                        | 13.77                | 38                             |
| A1142             | 25                   | 1                    | 0.596      | 15                        | 1.606                | 24                             |
| A1173             | 28                   | 110                  | 20.96      | 27                        | 30.45                | 25                             |
| A1190             | 65                   | 88                   | 9.149      | 63                        | 9.896                | 55                             |
| A1205             | 46                   | 67                   | 9.111      | 42                        | 11.84                | 43                             |
| RXCJ1115.5+5426   | 52                   | 50                   | 6.798      | 45                        | 10.48                | 43                             |
| SHK352            | 44                   | 24                   | 3.063      | 32                        | 6.125                | 35                             |
| A1314             | 37                   | 5                    | 1.151      | 33                        | 1.832                | 33                             |
| A1377             | 47                   | 48                   | 6.697      | 50                        | 5.913                | 47                             |
| A1424             | 49                   | 45                   | 8.575      | 39                        | 13.47                | 43                             |
| A1436             | 46                   | 51                   | 15.6       | 64                        | 8.021                | 58                             |
| MKW4              | 26                   | 1                    | 0.1811     | 19                        | 0.5456               | 19                             |
| RXCJ1210.3+0523   | 30                   | 67                   | 25.68      | 36                        | 19.22                | 38                             |
| Zw1215.1+0400     | 82                   | 62                   | 10.46      | 90                        | 7.965                | 74                             |
| A1552             | 70                   | 113                  | 15.72      | 78                        | 11.33                | 66                             |
| A1663             | 68                   | 86                   | 7.363      | 55                        | 12.23                | 51                             |
| MS1306            | 22                   | 104                  | 34.78      | 19                        | 44.83                | 21                             |
| A1728             | 46                   | 135                  | 11.93      | 22                        | 26.7                 | 33                             |
| RXJ1326.2+0013    | 16                   | 118                  | 34.21      | 12                        | 57.11                | 17                             |
| MKW11             | 13                   | 8                    | 1.927      | 9                         | 4.284                | 10                             |
| A1750             | 58                   | 86                   | 16.57      | 71                        | 12.32                | 59                             |
| A1767             | 90                   | 35                   | 3.314      | 59                        | 6.624                | 54                             |
| A1773             | 52                   | 90                   | 12.51      | 49                        | 15.08                | 45                             |
| RXCJ1351.7+4622   | 18                   | 31                   | 25.54      | 29                        | 13.96                | 35                             |
| A1809             | 63                   | 121                  | 16.62      | 67                        | 11.66                | 56                             |
| A1885             | 29                   | 74                   | 9.011      | 21                        | 50.58                | 20                             |
| MKW8              | 19                   | 8                    | 2.823      | 17                        | 3.39                 | 19                             |
| A2064             | 30                   | 47                   | 11.97      | 22                        | 21.44                | 29                             |
| A2061             | 95                   | 80                   | 5.412      | 85                        | 7.381                | 69                             |
| A2067             | 24                   | 128                  | 37.06      | 28                        | 24.3                 | 31                             |
| A2110             | 39                   | 176                  | 21.44      | 32                        | 34.32                | 33                             |
| A2124             | 70                   | 29                   | 2.492      | 48                        | 6.036                | 47                             |
| A2142             | 141                  | 115                  | 10.83      | 186                       | 6.141                | 113                            |
| NGC6107           | 28                   | 10                   | 2.195      | 22                        | 4.034                | 22                             |
| A2175             | 49                   | 77                   | 35.08      | 71                        | 14.64                | 66                             |
| A2197             | 35                   | 3                    | 1.814      | 63                        | 0.8029               | 59                             |
| A2199             | 77                   | 0                    | 0.3236     | 88                        | 0.239                | 75                             |
| A2245             | 94                   | 80                   | 6.411      | 88                        | 8.376                | 73                             |
| A2244             | 99                   | 112                  | 11.9       | 99                        | 11.75                | 82                             |
| A2255             | 167                  | 60                   | 3.933      | 173                       | 3.514                | 121                            |
| NGC6338           | 26                   | 2                    | 0.3734     | 16                        | 1.068                | 19                             |
| A2399             | 47                   | 48                   | 10.82      | 56                        | 7.135                | 51                             |
| A2428             | 37                   | 154                  | 18.16      | 33                        | 25.2                 | 33                             |
| A2670             | 95                   | 41                   | 9.163      | 109                       | 4.442                | 93                             |

of very low richness (it has only two galaxies brighter than the adopted luminosity limit), far lower than the other clusters in the sample. The list of the 53 remaining clusters is given in Table 1. We emphasize that only two cluster pairs have been removed from

the original sample because of their morphology; all the other excluded clusters have been removed because they are not fully enclosed in the sky area observed by SDSS or have suspect masses because the CIRS algorithm converged on a secondary clump.

Basically, we want to count red members within a specified luminosity range and colour and within a given cluster-centric radius, typically  $r_{200}$ , as is already done for other clusters at similar redshift (e.g. Andreon et al. 2006b) or in the distant universe (Andreon 2006, 2008; Andreon et al. 2008b). We only consider red galaxies because these objects are those whose luminosity evolution is better known and because their star formation rate (and therefore luminosity) cannot be altered by cluster merging, these objects having already exhausted the baryonic reservoir needed to form new stars.

Since we aim to replicate the present analysis to include additional clusters in future papers, we take a (passive evolving) limiting magnitude of  $M_V = -20$  mag, which is the approximate completeness of the SDSS at  $z = 0.3$  and of the CFHTLS wide survey and CTIO imaging (e.g. Andreon et al. 2004) of the XMM-LSS field at  $z \sim 1$ ; it is also a widely used magnitude cut (e.g. De Lucia et al. 2007; Andreon 2008, etc.). Magnitudes are passively evolving, modelled with a simple stellar population of solar metallicity, Salpeter IMF, from Bruzual & Charlot (2003), as in De Lucia et al. (2007) and Andreon (2008) amongst others. Such a correction is applied for consistency with other (past and future) work, but is actually unnecessary for our clusters because it is negligible given the small redshift range ( $0.03 < z < 0.1$ ) probed in this work.

We count only red galaxies, defined as those within 0.1 redward and 0.2 blueward in  $g - r$  of the colour–magnitude relation. This definition of ‘red’ is quite simple because for our cluster sample the resulting number hardly depends on the details of the ‘red’ definition; the determination of the precise location of the colour–magnitude relation is irrelevant because the latter is much narrower than 0.3 mag and because practically all galaxies brighter than the adopted luminosity cut are red. Colours are corrected for the colour–magnitude slope, but again this is a negligible correction given the small magnitude range explored (a couple of magnitudes). For the colour centre, we took the peak of the colour distribution.

Some of the galaxies counted in the cluster line of sight, are actually in the cluster fore/background. The contribution from background galaxies is estimated, as usual, from a reference direction (e.g. Zwicky 1957; Oemler 1974; Andreon, Punzi & Grado 2005). The reference direction is taken outside the turnaround radius, or for the few clusters too close or near to an SDSS border, near the turnaround radius.

Since richness is based on galaxy counts, it is computed within a cylinder of radius  $r_{200}$ . Masses are instead calculated (by Rines & Diaferio 2006) within spheres of radius  $r_{200}$ .

Table 1 gives for our 53 clusters: (1) the cluster id; (2) the observed number of galaxies in the cluster line of sight within  $r_{200}$ ,  $obstot_i$ ; (3) the observed number of galaxies in the reference line of sight,  $obsbkg_i$ ; (4) the ratio between the cluster and reference solid angles,  $C_i$ . Columns 5 and 6 list  $obstot_i$  and  $C_i$ , but for the radius inferred using equation (18), introduced in Section 7.1, based on the observed number of galaxies, within an aperture of  $1 h^{-1}$  Mpc,  $obsn(<1.43)$ . Column 7 lists  $obsn(<1.43)$ .

## 6 RESULTS

### 6.1 Richness–mass model

The aim of this section is to present a Bayesian analysis of the richness–mass model. In particular, we wish to acknowledge the uncertainty in all the measurements, including in error estimates. Most previous approaches assume that errors are perfectly known, which is seldom the case for astronomical measurements, in particular for complex astronomical measurements such as caustic masses

and velocity dispersions, whose quoted errors come from a simplified analysis. Furthermore, no regression method for a Poisson quantity has been previously published in astronomical journals and even less so for a difference of Poisson deviates.

First of all, because of errors, observed and true values are not identically equal. The variables  $n200_i$  and  $nbg_i$  represent the true richness and the true background galaxy counts in the studied solid angles. We measured the number of galaxies in both cluster and control field regions,  $obstot_i$  and  $obsbkg_i$  respectively, for each of our 53 clusters (i.e. for  $i = 1, \dots, 53$ ). We assume a Poisson likelihood for both and that all measurements are conditionally independent. The ratio between the cluster and control field solid angles,  $C_i$ , is known exactly. In formulae:

$$obsbkg_i \sim \mathcal{P}(nbg_i), \quad (5)$$

$$obstot_i \sim \mathcal{P}(nbg_i/C_i + n200_i). \quad (6)$$

For each cluster, we have a cluster mass measurement and a measurement of the error associated with this mass,  $obslgM200_i$  and  $obserrlgM200_i$ , respectively. We assume that the likelihood model is a Gaussian centred on the true value of the cluster mass,  $lgM200_i$ , with a scatter given by the true value of the mass error,  $\sigma_i$ :

$$obslgM200_i \sim \mathcal{N}(lgM200_i, \sigma_i^2). \quad (7)$$

We now need to address the fact that we do not know the true value of the mass error and that we only have an estimate of it, i.e. we need to model the relationship between  $\sigma_i$  and  $obserrlgM200_i$ . We use a scaled  $\chi^2$  distribution, chosen so that  $obserrlgM200_i^2$  will be unbiased for  $\sigma_i^2$ , with the (welcome) additional property that positivity is enforced:

$$obserrlgM200_i^2 \sim \sigma_i^2 \chi_\nu^2 / \nu. \quad (8)$$

Notice that for mathematical reasons we model the relationship between variances rather than between standard deviations. The degrees of freedom of the distribution,  $\nu$ , control the spread of the distribution, with large  $\nu$  meaning that quoted errors will be close to true errors. Our baseline analysis uses  $\nu = 6$  to quantify that we are 95 per cent confident that quoted errors are correct up to a factor of 2 (i.e. that  $\frac{1}{2} < \frac{obserrlgM200_i^2}{\sigma_i^2} < 2$ , derived via the equivalent probability statement for  $obserrlgM200_i^2$  and  $\sigma_i^2$ ). We note that when  $\nu = 6$ , the  $\chi^2$  distribution is quite skewed, and most of the remaining 5 per cent probability lies below 1/2. We anticipate that results are relatively robust to the choice of  $\nu$ . The shape of the adopted distribution, a  $\chi^2$  distribution, is for analogy to the case in which the quoted error is derived as a result of repeated observations; in such a case, standard sampling theory for Gaussian data would have made our choice extremely natural.

We now turn to the unobserved quantities in our model, for which we will specify independent prior distributions. We assume a linear relation between the unobserved mass and  $n200$  on the log scale, with intercept  $\alpha + 14.5$ , slope  $\beta$  and intrinsic scatter  $\sigma_{scat}$ :

$$lgM200_i \sim \mathcal{N}(\alpha + 14.5 + \beta(\log(n200_i) - 1.5), \sigma_{scat}^2). \quad (9)$$

Note that  $\log(n200)$  is centred at an average value of 1.5 and  $\alpha$  is centred at  $-14.5$ , purely for computational advantages in the MCMC algorithm used to fit the model (it speeds up convergence, improves chain mixing, etc.). Please note that the relation is between true values, not between observed values, which may be biased, as we will show in Appendix A for an astronomical sample affected by Malmquist bias.

The priors on the slope and the intercept of the regression line in equation (9) are taken to be quite flat, a zero-mean Gaussian with very large variance for  $\alpha$  and a Student's  $t$  distribution with 1 degree of freedom for  $\beta$ . The latter choice is made to avoid that properties of galaxy clusters depend on astronomers rules to measure angles (from the  $x$  or from the  $y$  axis). This agrees with the model choices in Andreon et al. (2006a and later works) but differs from some previous works (e.g. Kelly 2007) that instead assume a uniform prior on the slope  $\beta = \tan b$  and, as a consequence, favour some angles over others, depending on the adopted convention on the way angles are measured (i.e. from the  $x$  axis counter-clockwise as in mathematics, or from the  $y$  axis clockwise as in astronomy). Our  $t$  distribution on  $\beta$  is mathematically equivalent to an uniform prior on the angle  $b$ .

$$\alpha \sim \mathcal{N}(0.0, 10^4), \quad (10)$$

$$\beta \sim t_1. \quad (11)$$

For the true values of the cluster richness and background, we have tried not to impose strong a priori values, only enforcing positivity. Both are given independent improper uniform priors:

$$n200_i \sim \mathcal{U}(0, \infty), \quad (12)$$

$$nbkg_i \sim \mathcal{U}(0, \infty). \quad (13)$$

Finally, we need to specify the prior on the mass error,  $\sigma_i$ , and on the intrinsic scatter of the mass–richness scaling,  $\sigma_{\text{scat}}$ . These are positively defined (by definition), but otherwise we impose quite weak prior information. For mathematical reasons, we parametrize these priors on the variance rather than on the standard deviations as might seem more natural (for astronomers). An extremely common choice is the Gamma distribution:

$$1/\sigma_i^2 \sim \Gamma(\epsilon, \epsilon), \quad (14)$$

$$1/\sigma_{\text{scat}}^2 \sim \Gamma(\epsilon, \epsilon), \quad (15)$$

with  $\epsilon$  taken to be a very small number. The above equations translate almost literally into the JAGS code given in Appendix B. The code is only about 15 lines long in total, about two orders of magnitude shorter than any previous implementation of a regression model (e.g. Andreon et al. 2006a; Kelly 2007), none of which addresses the noisiness of the quoted error.

Our model seems quite complex with a lot of assumptions, more than other models adopted in previous analyses, but actually it makes weaker assumptions, plainly states what is actually also assumed by other models (e.g. the conditional independence and Poisson nature of  $obsbkg_i$  and  $obstot_i$ , the positivity of the intrinsic scatter, etc.) and removes approximations adopted in other approaches. For example, it is common to ignore the uncertainty in the count data and to take  $n200$  to be the observed  $obsn200 = obstot - obsbkg/C$ . However, doing so does not respect the fact that  $n200$  must be non-negative and in the low count regions  $obstot - obsbkg/C$  can be found to be negative (see Appendix B of Andreon et al. 2006a). Instead, we account for the difference and we will show in Appendix A an example of the danger of ignoring the difference between  $obsn200$  and  $n200$ . Equations (5) and (6) also capture the Poisson nature of galaxy counts that, for small values, is fairly different from the usual Gaussian approximation widely adopted in regression models published in astronomical journals. Furthermore, it is common to ignore the uncertainty in the mass error. Our model may easily recover this case, by letting  $\nu$  take a large value (formally, to go to infinity). Our model replaces this strong

assumption with a weaker one, namely that the quoted squared error is an unbiased measure of the true squared error. Finally, the remaining ingredients are just uniform (or nearly so) distributions in the appropriate space.

Essentially, our model assumes that the true richness and true mass are linearly related (with some intrinsic scatter) but, rather than having these true values, we have noisy measurements of both richness and scatter, with noise amplitude different from point to point. In the statistics literature, such a model is known as an ‘errors-in-variables regression’ (Dellaportas & Stephens 1995). Our model goes one step beyond the works of D’Agostini (2004), Andreon et al. (2006a) and Kelly (2007), which all assume errors to be perfectly known (and none of which deals with Poisson processes as galaxy counts). These works were, in turn, less approximate approaches than previous fitting methods used in astronomy to regress two quantities (for example, simple least-squares, bivariate correlated error and intrinsic scatter, etc.).

To summarize, the novelty of the present approach is to treat in a symmetric way measurements and estimates of errors. The parameters of primary importance are those of the linear relationship between true mass and richness, with associated intrinsic scatter  $\sigma_{\text{scat}}$  being of particular interest.

## 6.2 Richness–mass result

Using the model above, we found, for our sample of 53 clusters:

$$\lg M200 = (0.96 \pm 0.15)(\log n200 - 1.5) + 14.36 \pm 0.04. \quad (16)$$

(Unless otherwise stated, results of the statistical computations are quoted in the form  $x \pm y$ , where  $x$  is the posterior mean and  $y$  is the posterior standard deviation.)

Fig. 2 shows the scaling between richness and mass, observed data, the mean scaling (solid line) and its 68 per cent uncertainty (shaded yellow region) and the mean intrinsic scatter (dashed lines) around the mean relation. The  $\pm 1$  intrinsic scatter band is not expected to contain 68 per cent of the data points, because of the presence of measurement errors.

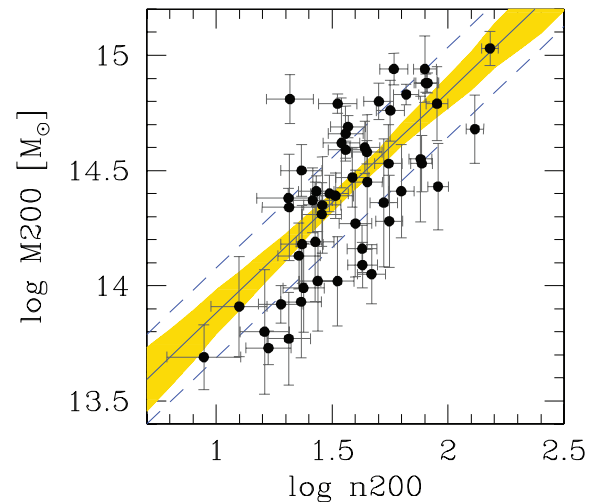


**Figure 2.** Richness–mass scaling. The solid line marks the mean fitted regression line of  $\lg M200$  on  $\log(n200)$ , while the dashed line shows this mean plus or minus the intrinsic scatter  $\sigma_{\text{scat}}$ . The shaded region marks the 68 per cent highest posterior credible interval for the regression. Error bars on the data points represent observed errors for both variables. The distances between the data and the regression line is due in part to the measurement error and in part to the intrinsic scatter.

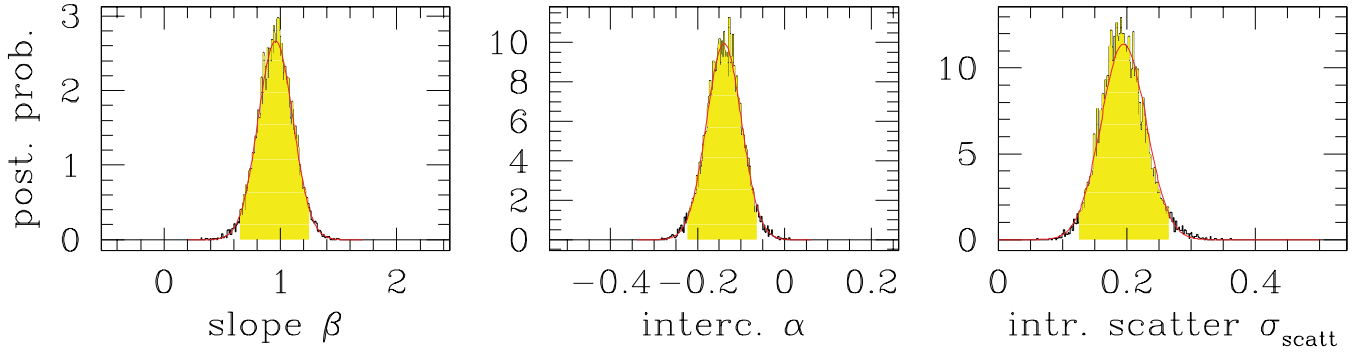


**Figure 3.** Posterior probability distribution for the parameters of the richness–mass scaling. The black jagged histogram shows the posterior as computed by MCMC, marginalized over the other parameters. The red curve is a Gauss approximation of it. The shaded (yellow) range shows the 95 per cent highest posterior credible interval.

Fig. 3 shows the posterior marginals for the key parameters; for the intercept, slope and intrinsic scatter  $\sigma_{\text{scat}}$ . These marginals are reasonably well approximated by Gaussians. The intrinsic mass scatter at a given richness,  $\sigma_{\text{scat}} = \sigma_{\lg M_{200} | \lg n_{200}}$ , is small,  $0.19 \pm 0.03$ . The small scatter and its small uncertainty is promising from the point of view of using  $n_{200}$  for cosmological aims, for example to estimate the mass distribution, given the *obsn*<sub>200</sub> distribution.

The slope between richness and mass is very near to 1 (within one-third of the estimated standard deviation), i.e. clusters that have twice as many galaxies are twice as massive.

### 6.3 Checks

First, our results are robust to the choice of  $\nu$  (we tested  $\nu = 6$  versus  $\nu = 3, 30, 300$  or  $\nu = 3000$ ).

Second, the determination of the slope of the richness scaling requires setting two (astronomical) parameters, a radius within which galaxies should be counted and a limiting (reference) magnitude. To investigate the dependence of the richness–mass slope on which limiting magnitude is adopted, we recompute  $n_{200}$  using two different limiting magnitudes, 1 and 2 mag deeper than our reference mag,  $M_V = -20$  mag. The resulting slopes of the mass–richness scaling are  $0.98 \pm 0.15$  and  $0.95 \pm 0.16$ , both very close to the original slope derived using the reference mag ( $0.96 \pm 0.15$ ). The intrinsic scatter changes insignificantly, by 0.01 dex, with the limiting magnitude.

We now check whether the scaling of richness found with mass may be biased (tilted) by having hypothetically taken a systematically incorrect  $r_{200}$  (for example, too small an  $r_{200}$  at large masses, or too big a one at small masses). Fig. 4 plots  $r_{200}$  as a function of cluster velocity dispersion. The superimposed straight line comes from assuming that  $r_{200}$  is the virial radius (i.e.  $M_{200} = M_{\text{virial}}$ ),  $r_{200} \propto s$  [e.g. equation (1) in Andreon et al. 2005; equation (1) in Carlberg et al. 1997; equation (3.1) in Muzzin et al. 2007] rather than as a fit to these points. As the points are scattered roughly around the slope of the expected relation, we reject the possibility that the slope between richness and mass (or velocity dispersion) is biased because of a bad choice of the reference radius in which galaxies are counted (one that does not correctly scale with mass).

In summary,  $n_{200}$  tightly correlates with mass, with 0.19 dex intrinsic scatter. The slope is fairly robust to the choice of the reference magnitude, the uncertainty of error terms ( $\nu$ ) and the a priori range of mass errors. Furthermore, it is unbiased with respect to a (hypothetical) bad choice of the reference radius.

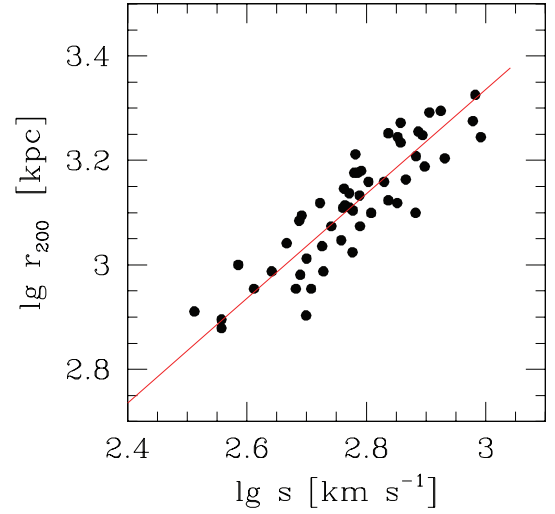


**Figure 4.**  $r_{200}$ – $s$  (velocity dispersion) scaling. The line marks the expected scaling,  $r_{200} \propto s$ . The good agreement between the trend identified by the data and the expected scaling implies that there is no velocity dispersion (mass) dependent systematic bias on the adopted  $r_{200}$ .

### 6.4 Richness–velocity dispersion scaling and results

Velocity dispersions,  $s$ , are observationally more expensive than  $n_{200}$  but less expensive than caustic masses. They are also good tracers of the cluster mass (e.g. Biviano et al. 2006; Mandelbaum & Seljak 2007; Evrard et al. 2008). Since at high redshifts caustic masses are observationally prohibitive to calculate, from the perspective of testing the evolution of the richness scaling it is useful to calibrate the scaling between richness and velocity dispersion.

The statistical model employed is very similar to that described for the richness–mass scaling; essentially we only need to read ‘velocity dispersion’ where mass was written. Because velocity dispersion errors are easier to measure than mass errors, we adopt  $\nu = 50$ , i.e. we are 68 per cent confident that quoted errors are correct up to a factor 1.1 (i.e. within 10 per cent).

Because of the different measurement units, the intercept  $\alpha$  is now centred at 2.8 (for computational purposes in JAGS).

For our sample, we found

$$\lg s = (0.30 \pm 0.04)(\lg n_{200} - 1.5) + 2.77 \pm 0.01. \quad (17)$$

Fig. 5 shows the fitted scaling between richness and velocity dispersion, the observed data, the posterior mean scaling (solid line)

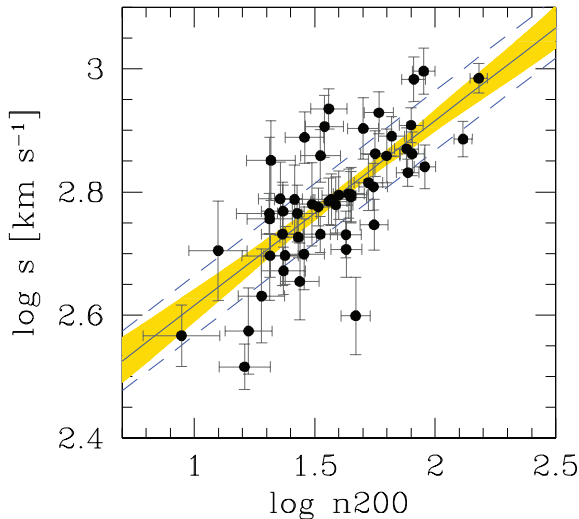


**Figure 5.** Velocity dispersion–richness scaling. Symbols are as in Fig. 2.

and its uncertainty (shaded yellow region) and the mean intrinsic scatter (dashed lines).

Similarly to the richness–mass scaling, the intercept, slope and intrinsic scatter have posterior marginals which are close to Gaussian. The intrinsic velocity dispersion scatter at a given richness,  $\sigma_{\text{scat}} = \sigma_{\log s | \log n200}$ , is small,  $0.05 \pm 0.01$ .

As in the case of the richness–mass scaling, these results are robust to the choice of  $\nu$ , for  $\nu \gtrsim 10$ .

The fitted slope of the richness–velocity dispersion scaling is one-third of the slope of the richness–mass scaling, as it should be, given that velocity dispersion scales with mass with power 0.33 (e.g. Evrard et al. 2008).

### 6.5 Caustic mass systematic errors

In the previous sections we have not accounted for possible systematic error in the caustic mass, except indirectly in a couple of locations: (a) in Fig. 4, when comparing the cluster velocity dispersion with  $r_{200}$ : if a systematic error on M200 were present, then the data would not scatter around the expected relation; (b) in Section 6.4, where we found that the slope of richness–velocity dispersion is one-third of the slope of the richness–mass, as expected for a mass that scales with the cube of velocity dispersion.

In order to further investigate the lack of gross systematic errors on caustic masses, we plot in Fig. 6 caustic masses against two masses, derived from velocity dispersion using relations calibrated with numerical simulations (left panel: Evrard et al. 2008, right panel: Biviano et al. 2006). The solid line is the one-to-one relation rather than a fit to the points. If caustic masses were systematically larger or smaller than masses derived from velocity dispersion, then these points might well be systematically above or below the solid line. If instead caustic masses were too big at high masses and too small at low masses, or vice versa, points should have a different (tilted) slope from the plotted line. Fig. 6 clearly shows that neither of the two cases occurs. A 30 per cent offset error or a 30 per cent tilt would be obvious to the eye. A second obvious conclusion coming from this figure is that the two panels are virtually indistinguishable. This is because the two calibrations of the velocity dispersion–mass relation, although independent, are actually almost identical.

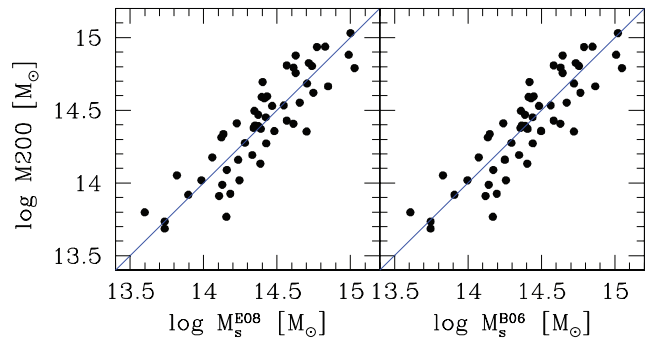


**Figure 6.** Caustic masses (ordinate) versus masses derived from the cluster velocity dispersion using relations calibrated with numerical simulations (left panel: Evrard et al. 2008, right panel: Biviano et al. 2006). The solid, slanted, line marks the equality and it is not a fit to the data.

To summarize, this section shows the lack of an obvious gross systematic error in caustic masses. ‘Statistical’ errors on caustic mass and noisiness of errors are built-in in our model.

## 7 RICHNESS AS MASS PROXY

The richness–mass scaling derived in previous sections needs a known  $r_{200}$ , the radius within which galaxies have to be counted. If we want to use  $n_{200}$  as a mass proxy,  $r_{200}$  should be instead considered as unknown. Lopes et al. (2009) disagree with this reasoning because in their work they measured the performance of mass proxies assuming  $r_{200}$  (or  $r_{500}$ ) known, when instead it is unknown for clusters with unknown masses. We now measure the performances of a richness estimate that does not require the knowledge of  $r_{200}$ , counting galaxies within some reference radius,  $\widehat{r}_{200}$ , that can be measured from imaging data.<sup>5</sup> Since there are a number of ways  $\widehat{r}_{200}$  may be estimated, we consider some of them.

In principle, we may be interested in the following.

(a)  $\sigma_{\text{scat}}$ , i.e. the intrinsic scatter in mass at a given richness. This may be of interest to those who want to know which part of the observed scatter is intrinsic.

(b) The uncertainty of the mass estimated from the cluster richness. This is, for example, the case when one has one or a few clusters with a measurement of richness and we would like to know their estimated mass. With real data, cluster richness is known with a finite precision which induces a minimal floor in the performances of richness as mass proxy.

To this end, we first need to find a way to estimate  $\widehat{r}_{200}$  from galaxy counts, because clusters for which we want an estimate of mass will not have a known  $r_{200}$ . Then we will calibrate the measured  $\widehat{n}_{200}$  ( $n_{200}$  values within  $\widehat{r}_{200}$ ) with mass and estimate the uncertainty of the predicted  $\log M_{200}$  for a cluster sample, the latter using equation (4). Recall that the performance of richness as a mass predictor accounts for all terms entering into the modelling of proxy and mass, which include the uncertainty of the proxy value and the uncertainty on the parameters describing the regression between mass and mass proxy (slope, intercept, intrinsic scatter and their covariance).

As in some literature approaches, we use the same sample both to establish the scaling between regressed quantities and to

<sup>5</sup> The hat above symbols is introduced to distinguish these values, derived from equation (18), from values used in previous sections which were taken from CIRS.

measure the proxy performance. However, these literature approaches compute the proxy performances from a single regression (usually named the best fit, i.e. for a single value of  $\theta$ ), ignoring that other fits are similarly acceptable and that the best fit itself is uncertain (i.e. ignoring uncertainties on slope, intercept and intrinsic scatter). When the best fit scaling is defined as the one minimizing the scatter (and this is not our case), the measured scatter underestimates the true scatter, by definition. Our approach supersedes these previous approaches, allowing for errors other approaches neglect and also including their covariance.

### 7.1 Reference case

Since we do not know a priori which approach is the optimal way to estimate  $r_{200}$  from imaging data alone, in this section we consider a reference case and in the following section we make a number of tests to see how robust are our conclusions to the assumptions made in the reference case.

We simply compute the number of cluster galaxies (i.e.  $obstot - obsbkg/C$ ) within a radius of 1.43 Mpc,  $obsn(r < 1.43)$  and then we estimate  $\widehat{r}_{200}$  as

$$\log \widehat{r}_{200} = 0.6(\log obsn(r < 1.43) - 1.5). \quad (18)$$

The slope, 0.6, and the radius, 1.43 Mpc, are taken for consistency with Koester et al. (2007a). The intercept is chosen to reproduce the trend between known  $obsn(r < 1.43)$  and  $r_{200}$  radii. Therefore, our  $\widehat{r}_{200}$  has no bias (or at most a negligible one) with respect to  $r_{200}$  by construction. Instead, the normalization (intercept) adopted in Koester et al. (2007a) has been later discovered (Becker et al. 2007; Johnston et al. 2007) to give radii too large by a factor of 2.

Having adopted the radius above, we need to count the galaxies within this radius and recompute the solid angle ratio. Asymptotically,  $\widehat{n}_{200}$  is given by  $\widehat{obstot} - obsbkg/\widehat{C}$ , but our analysis does not assume that this asymptotic behaviour holds within our finite sample.<sup>6</sup>

Using our fitting model, we found

$$\lg M_{200} = (0.57 \pm 0.15)(\log \widehat{n}_{200} - 1.5) + 14.40 \pm 0.05. \quad (19)$$

The data and fit are depicted in Fig. 7. The major difference with respect to our fit performed on measurements using knowledge of  $r_{200}$  (i.e. Section 6.2) is the shallower slope, which is 1.9 combined  $\sigma$  shallower than it was. Intercept, slope and intrinsic scatter have posteriors close to Gaussian. The intrinsic scatter is small, it has mean  $0.27 \pm 0.03$  dex. With respect to the case where  $r_{200}$  is known, the intrinsic scatter is larger ( $0.27 \pm 0.03$  versus  $0.19 \pm 0.03$ ), as expected because we are not using our knowledge about  $r_{200}$ . We emphasize that this is the uncertainty on the mass inferred from  $\widehat{n}_{200}$  if we were able to measure the latter quantity with very large precision, being 0.27 dex the part of the mass scatter not associated to measurement errors. Since  $\widehat{n}_{200}$  is not better known than allowed by the observed data, the mass error inferred from a (noisy) estimate of the cluster richness is larger and is given by the average uncertainty of predicted  $\lg M_{200}$ , which is found to be  $0.29 \pm 0.01$  dex. Therefore, we can predict the mass of a cluster within 0.29 dex by measuring its richness. Since the uncertainty on the predicted mass is only slightly larger than the intrinsic scatter, the uncertainty on the mass–richness scaling (regression) and the proxy uncertainty only account for small amounts of the variability.

<sup>6</sup> Background counts do not need to be recomputed, which is why there is no hat on  $obsbkg$ .

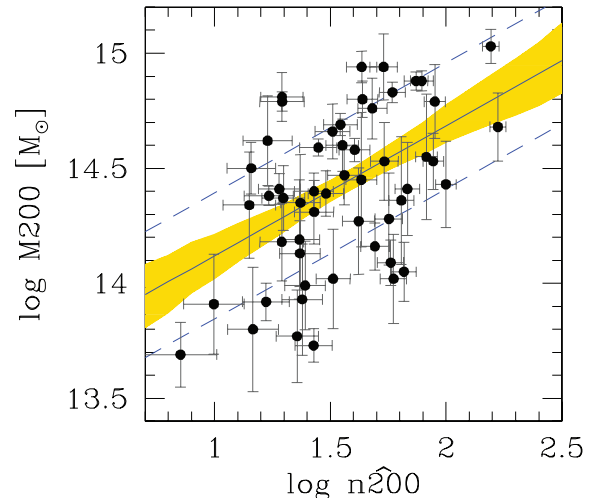


**Figure 7.** Richness–mass scaling for a richness measured within  $\widehat{r}_{200}$ , an  $r_{200}$  radius estimated from optical data. Symbols are as in Fig 2.

Therefore, the performance of richness as mass proxy is dominated by the mass scatter at a given richness.

In comparison to caustic cluster masses, which have, on average, a 0.14 dex error, masses estimated from  $\widehat{n}_{200}$  have twice worse accuracy (0.29 versus 0.14 dex). Although  $\widehat{n}_{200}$  is noisier mass proxy than caustic masses, the former requires far less expensive observations than the latter and as a consequence is available for almost a 200 times larger sample. The last number is computed as the ratio of the number of clusters with available richness from SDSS (e.g. maxBCG clusters, about 13 000, Koester et al. 2007a) with those with caustic masses in the same sky region (74, listed in Rines & Diaferio 2006).

### 7.2 Other paths to $\widehat{n}_{200}$

To check the resulting robustness of our results to the few parameters involved in the computation, we make some tests. First, we take as reference radius a value near to the average of our  $r_{200}$ , 1.25 Mpc and use  $obsn(< 1.25)$  as pivot value for estimating  $\widehat{r}_{200}$ . Second, we changed the slope to 0.55, because some maxBCG papers (Hansen et al. 2005; Becker et al. 2007; Koester et al. 2007b) disagree on the slope value (0.55 or 0.6) adopted in Koester et al. (2007a). Third, we decide to count galaxies in a radius twice larger than  $\widehat{r}_{200}$ , to check the sensitivity to the adopted reference radius. The factor 2 is adopted to follow the maxBCG papers, which adopted an  $r_{200}$  radius later discovered to be too large by a factor of 2. Fourth, we consider the simplest case, we adopt a fixed aperture, 1.43 Mpc, for all clusters, irrespective of their size or mass. In all these cases we found similar slopes, intrinsic mass scatter and average uncertainty of predicted  $\lg M_{200}$  as in our reference case. This is expected, given that the intrinsic scatter alone accounts for most of the uncertainty of predicted masses.

In summary, if  $r_{200}$  has to be estimated from a scaling relation based on counting red galaxies within aperture in imaging data, it seems that we have reached a floor on the quality of mass determination, 0.27 dex of intrinsic scatter and 0.29 dex of average uncertainty of predicted  $\lg M_{200}$ , no matter how precisely  $\widehat{r}_{200}$  is defined.

### 7.3 Comparison with other mass proxies

In this section we want to compare the performances of the X-ray luminosity and richness as mass proxies. Among all possible proxies, we choose X-ray luminosity because it is measurable from survey data, as is richness. Other mass proxies, such as  $Y_X$ , do require follow-up observations and it would be unwise to compare them to (optical) mass estimates derived from survey data. Of course, in this comparison, both mass proxies are measured without using knowledge of mass or linked quantities, such as  $r_{200}$ , because they are unknown for clusters with unknown masses. Lopes et al. (2009) disagree with this reasoning because they measured and compared the performance of mass proxies assuming knowledge of  $r_{200}$  (or  $r_{500}$ ).

Richness and its performance as a mass predictor have been measured by us in the previous section. In short, richness offers a mass with a 0.29 dex uncertainty. X-ray luminosities are collected by Rines & Diaferio (2006) and come, in order of preference, from the ROSAT-ESO Flux-Limited X-Ray (REFLEX), the Northern ROSAT All-Sky galaxy cluster survey (NORAS), the Bright Cluster Survey (BCS) and its extension (eBCS) and, finally, from the X-Ray Brightest Abell Cluster Survey (XBACS). Rines & Diaferio (2006) do not list errors for X-ray luminosities, therefore we repeated our analysis with a 5 per cent and a 30 per cent error and found that results are robust to the adopted error. The model for the logarithm of the X-ray flux is assumed to be Gaussian and the equations

$$\text{obs} \lg L_{X_i} \sim \mathcal{N}(\lg L_{X_i}, \text{err}^2), \quad (20)$$

$$\lg L_{X_i} \sim \mathcal{U}(0, \infty), \quad (21)$$

$$\lg M_{200_i} \sim \mathcal{N}(\alpha + 14.5 + \beta(\lg L_{X_i} - 42.5), \sigma_{\text{scat}}^2) \quad (22)$$

replace equations (5), (6), (9), (12) and (13). Before proceeding further, we emphasize that our analysis involving  $L_X$  ignores the Malmquist bias due to the X-ray selection of the cluster sample (e.g. Stanek et al. 2006), i.e. clusters brighter than average for their mass are over-represented (easier to detect and thus more likely to be in the sample).

Fig. 8 shows richness versus mass and X-ray luminosity versus mass, the fitted scaling (posterior mean, solid line) and the mean

model plus and minus the uncertainty of predicted masses (dashed lines).

By eye, our fit seems shallower than the data suggest. Our derived slopes match those derived by other fitting algorithms; for example, the  $L_X$  versus mass regression has a slope of  $0.30 \pm 0.10$  using our fitting algorithm, a slope of  $0.29 \pm 0.10$ , neglecting the uncertainty on the error (i.e. following Andreon 2006 and Kelly 2007) and a BCES( $Y|X$ ) (Akritas & Bershady 1996) slope of  $0.31 \pm 0.07$ . This slope is theoretically different from the slope of the underlying relation between these quantities because we are interested here in something different, namely prediction as explained in Section 4. As a further cautionary check, we verified that the uncertainty of predicted masses, the quantity of interest here, is robust, in particular we forced a steeper slope (e.g. we keep the  $L_X$ -mass slope to 0.5), getting an identical value for the uncertainty.

For the richness, we found (Section 7.1) a mass uncertainty of  $0.29 \pm 0.01$  dex. For the  $L_X$  proxy, we found an identical value for the mass uncertainty,  $0.30 \pm 0.01$  dex. Therefore, masses predicted by  $L_X$  or richness are comparably precise, to about 0.30 dex. Qualitatively, one may reach the same conclusion by inspecting Fig. 8 and performing an approximate analysis requiring a number of assumptions that are unnecessary in our statistical analysis; the precision of a mass proxy is, in our case, dominated by the intrinsic scatter in mass at a given proxy value, which in turn is not too dissimilar from the vertical scatter in Fig. 8 because observational mass errors are not large. The two data point clouds display similar widths at a given value of the proxy (see Fig. 8) and therefore the two proxies display similar performances as mass predictors. Our statistical analysis removes approximations and holds when the qualitative analysis does not, for example if the regression is poorly determined or the mass errors are large or the richness is poorly determined or in the presence of a mismatch in proxy value between clusters with known and to-be-estimated mass.

A plot similar to our Fig. 8 by Borgani & Guzzo (2001) seems to show a better  $L_X$  performance, but only when compared to an optical richness estimated by eye (Abell 1958; Abell, Corwin & Olowin 1989).

The fact that the studied sample is mainly (but not exactly), an X-ray flux-limited sample gives an advantage to  $L_X$  as a mass proxy; had we taken a volume complete mass-limited sample of the same cardinality in the same Universe volume (i.e. unbiased with mass) instead of the adopted (almost) flux-limited sample, some clusters

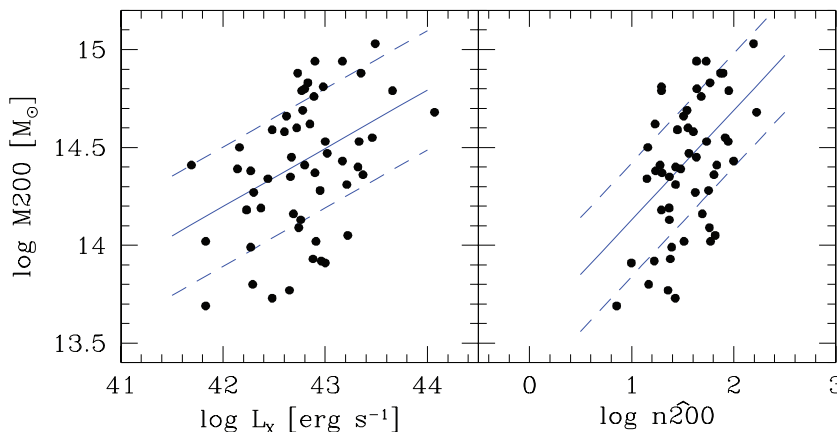


**Figure 8.** Comparison of the performances, as mass predictor, of X-ray luminosity and richness. The solid line marks the mean model; the dashed lines delimit the mean model plus and minus the average uncertainty of predicted masses. Equal ranges (3.5 dex) are adopted for richness and X-ray luminosity. See Section 4 for a discussion of the slopes of prediction lines.

would not be X-ray detected and thus would have a very loose mass constraint, lacking an  $L_X$  detection. A richness-selected sample formed by all clusters with  $n_{200}$  above a threshold would also have favoured the  $n_{200}$  mass proxy, because the scatter between  $n_{200}$  and  $L_X$  would have included in the sample clusters undetected in X-ray. Therefore, in spite of the selection favouring the X-ray proxy, richness performs as  $L_X$  in predicting cluster masses.

Richness has a further advantage, it is available for a larger number of clusters per unit Universe volume. Let us consider, for example,  $z < 0.3$ , clusters with optical estimates of mass (i.e. with  $n_{200}$ ) outnumber the one with an X-ray-based proxy (i.e. with  $L_X$ ) by a factor of 58; there are 5800  $\text{ster}^{-1}$  optically detected clusters (maxBCG clusters, Koester et al. 2007a) and only 100  $\text{ster}^{-1}$  X-ray detected (REFLEX clusters, Böhringer et al. 2001). The optically selected cluster sample is a quasi-volume-limited sample. If, mimicking what has been done for X-ray measurements, a cut on  $\widehat{n_{200}}$  signal to noise is used, instead of adopting a quasi-volume-limited sample, the number of optically detected clusters grows significantly. Similarly, in about four degrees squares, there are about 106 clusters with  $\text{obsn}_{200} > 6$  (Andreon et al., in preparation) and  $0.32 < z < 0.8$ . In the very same area there are nine C1 clusters (Pacaud et al. 2007), i.e. ten times fewer. If, as for X-ray data, a cut on  $\text{obsn}_{200}$  signal to noise is adopted, the number of optically detected clusters would be larger. Schuecker, Böhringer & Voges (2004) claim SDSS being deeper than the Rosat All Sky Survey (RASS) ‘can thus be used to guide a cluster detection in RASS down to lower X-ray flux limits’. Unsurprisingly, the fact that COSMOS (Scoville et al. 2007) and many X-ray cluster surveys keep X-ray detections that match with optical clusters (e.g. Finoguenov et al. 2007, for COSMOS) assumes that in current data sets X-ray clusters are a sub-set of optically selected clusters, i.e. a smaller sample. Finally, while X-ray-selected clusters are almost always optically detected, the reverse has proved much more difficult, which clarifies that optical cluster detection is observationally cheaper. Therefore, studies that require large samples of clusters or a denser sampling of the universe volume may adopt optically selected cluster samples because they offer a mass estimates of comparable quality for larger samples.

Some words of caution are in order. The good performance of richness as a mass estimator holds for our sample and should be confirmed on a sample of clusters optically selected. Of particular relevance is the frequency of catalogued optically selected clusters being instead line-of-sight superpositions of smaller systems. Such points will be addressed by our X-ray follow-up of all (53) clusters optically selected with  $59 < n_{200} < 70$  and  $0.1 < z < 0.3$  in the maxBCG catalogue (Koester et al. 2007a).

Similarly, the same caution is in order for other mass estimators. For example,  $L_X$  has been proposed as a mass estimator by Maughan (2007). Its performances as a mass predictor, however, have been measured on data having  $L_X$  based on hundreds or thousands of photons and therefore the noisiness of  $L_X$  itself in establishing his performances as a mass estimator has been largely underestimated. Furthermore, point sources are identified and removed through (high-resolution) Chandra observations, making the identification and flagging of point sources easy and studied clusters have preferentially large count rates and are little affected by residual, unrecognized as such, point sources. To summarize, the good performances of  $L_X$  cannot be immediately extrapolated to common cluster samples, dominated by objects with noisy  $L_X$ /count rate (because of the steep cluster number counts) and for which residual point source contamination is more important and which are perhaps observed by survey instruments as XMM, having a

lower resolutions and therefore a more difficult identification and of contaminating point sources.

## 8 A THIRD MASS CALIBRATION

Our approach can be used to calibrate richness against mass, no matter which mass we are talking about (e.g. lensing, caustic, Jean, etc). In Section 6.4 we use velocity dispersion (uncorrected with any numerical simulation) to calibrate the richness scaling, recycling the same model already used for caustic masses. As a further example, we recycle our model to calibrate richness against  $M_s$ , the mass derived from velocity dispersion,  $s$ , fixed with a mass– $s$  relation derived by numerical simulations. We adopt the mass– $s$  relation in Biviano et al. (2006). As shown in Fig. 6, had we used the mass– $s$  relation in Evrard et al. (2008) we would have found near-indistinguishable results. To use the masses  $M_s$  in place of the caustic ones, we need only write their values (and their errors) in the data file and run our same model. Mass errors are derived by combining in quadrature velocity dispersion errors (converted to mass) and the intrinsic noisiness of  $M_s$  (12 per cent, from Biviano et al. 2006). We adopt, as for velocity dispersions,  $v = 50$  (but results do not depend on  $v$ , if  $v \gtrsim 30$ ). We found, for our sample of 53 clusters:

$$\lg M_s = (0.92 \pm 0.11)(\log n_{200} - 1.5) + 14.35 \pm 0.03$$

with an intrinsic scatter of  $0.12 \pm 0.04$  dex. The intercept, slope and intrinsic scatter have posterior marginals that are close to Gaussian, as for the scaling with caustic masses.

Unsurprisingly, we found a near-identical slope and intercept to those using caustic masses; to find different values, we would need that caustic masses be tilted or offset from velocity-dispersion-derived masses, whereas Fig. 6 shows the lack of a gross tilt or offset.

We also found compatible values for intrinsic scatter ( $0.12 \pm 0.04$  versus  $0.19 \pm 0.03$ ). The similarity of the two intrinsic scatters testifies that errors on caustic masses and on  $M_s$  are on a consistent scale, i.e. similarly correct (or incorrect); for example, if the caustic mass error is overestimated, the intrinsic scatter of the caustic mass–richness scaling would be lower than the one using  $M_s$ , because the intrinsic scatter is that part of the scatter does not account for measurement errors.

We now move on to consider  $\widehat{n_{200}}$ , the cluster richness estimated without knowledge of the cluster mass and linked quantities, as  $r_{200}$ . How does it perform as a mass proxy, when  $\lg M_s$  is used as mass? At the minimal effort of listing the data in the data file, we find:

$$\lg M_s = (0.62 \pm 0.12)(\log \widehat{n_{200}} - 1.5) + 14.40 \pm 0.04,$$

i.e. indistinguishable from the scaling with caustic masses,

$$\lg M_{200} = (0.57 \pm 0.15)(\log \widehat{n_{200}} - 1.5) + 14.40 \pm 0.05.$$

The intercept, slope and intrinsic scatter have posteriors close to Gaussian, as with the scaling with caustic masses. The intrinsic scatter is small, it has mean  $0.21 \pm 0.03$  dex, very similar to the one obtained using caustic masses,  $0.27 \pm 0.03$  dex. The average uncertainty of predicted  $\lg M_s$ , i.e. the quality of richness as mass proxy, is found to be  $0.23 \pm 0.01$ , similar to the one obtained using caustic masses,  $0.29 \pm 0.01$  dex.

To explore the quality of  $L_X$  as a mass proxy when mass is measured by  $\lg M_s$ , we only need to list the data and run our model, with no change. We found that mass, predicted from  $L_X$  has an average uncertainty of  $0.22 \pm 0.01$ . When caustic masses are used, the average uncertainty of predicted masses was  $0.30 \pm 0.01$ .

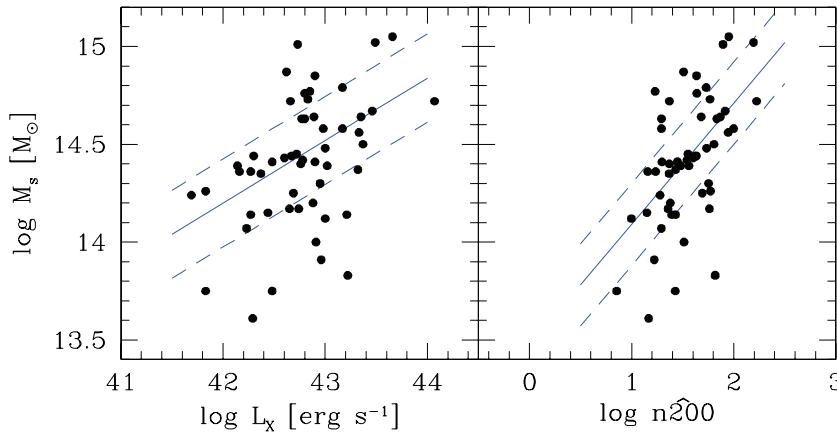


**Figure 9.** Comparison of the performances, as mass predictors, of X-ray luminosity and richness. In this figure we use masses inferred from cluster velocity dispersion, but the basic result does not change; X-ray luminosity and richness score similarly as mass proxies. Lines and symbols as in previous figure.

Fig. 9 shows the richness versus mass and X-ray luminosity versus mass, for velocity-dispersion-derived masses. It is the equivalent of Fig. 8. The bottom line is hardly different from that derived in Section 7.3; richness and X-ray luminosity show comparable performances in predicting cluster mass (either caustic or derived from cluster velocity dispersion). If anything, there is some tentative evidence that both X-ray luminosity and richness better predict masses derived from velocity dispersions than caustic masses ( $\sim 0.21$  versus  $\sim 0.29$ ). We will defer to a future paper for an in-depth examination of the significance of this possible effect.

## 9 DISCUSSION AND CONCLUSIONS

In order to exploit clusters as cosmological probes, it is important to know the mass–proxy scaling. Although self-solving for the scaling itself is feasible, an independent calibration of the scaling is a safety check and allows us to improve cosmological constraints.

In this paper we computed the richness (number of red galaxies brighter than  $M_V = -20$  mag) of 53 clusters with available caustic masses, the latter having the advantage that, unlike other masses, they do not require the cluster to be in dynamical or hydrostatic equilibrium. We investigated the possibility of systematic biases by comparing caustic masses to masses derived from velocity dispersions and found no gross offsets or tilt. Richness is computed from SDSS imaging data both with and without knowledge of the reference radius  $r_{200}$  from SDSS imaging data. We then measure the scaling between richness and caustic mass. Our richness–mass calibration is solid, both from an astrophysical perspective, because the masses we adopted are amongst the most hypothesis-parsimonious estimates of cluster mass, and statistically, because we account for terms usually neglected, such as the Poisson nature of galaxy counts, the intrinsic scatter and uncertain errors. Our cluster sample is larger, by a factor of a few, than previous samples used in comparable works. The data and code used for the stochastic computation are provided in this paper. This code is quite general; we used it to derive two alternative richness–mass calibrations, using as a mass proxy the cluster velocity dispersion or a mass calibrated from the velocity dispersion via numerical simulations.

We found a slope between richness and (caustic) mass of  $0.96 \pm 0.15$  with knowledge of  $r_{200}$ , i.e. clusters that have twice the number of galaxies are twice as massive. The intrinsic scatter is small, 0.19 dex. An identical result is found using masses calibrated from

the velocity dispersion via numerical simulations. When the reference radius in which galaxies should be counted has to be estimated from optical data, the slope decreases to  $0.57 \pm 0.15$  and masses inferred by the cluster richness are good to within  $0.29 \pm 0.02$  dex, largely independently of the way the radius itself is estimated. The uncertainty of predicted masses is twice the average uncertainty of caustic masses (0.14 dex), but observationally less expensive to obtain and for this reason available for a 200 times larger sample. Richness is a mass proxy of quality comparable to X-ray luminosity, both showing a 0.29 dex mass uncertainty, but is less observationally expensive than the latter, as testified by the larger number density of optically detected clusters with respect to X-ray detected clusters in current catalogues. This has important applications in the estimation of cosmological parameters from optical cluster surveys, because in current surveys clusters detected in the optical range outnumber, by at least one order of magnitude, those detected in X-ray. In particular, we note that our richness is computed from the shallowest data ever used by us, 54 s exposures at a 2-m telescope, taken under mediocre seeing conditions (1.5 arcsec FWHM), i.e. SDSS imaging data. Similar or better data should be available for every cluster; we are unaware of a cluster of galaxy claimed to be so without some optical imaging of it.

Similar performances of X-ray luminosity and richness in predicting cluster masses has been confirmed using cluster masses derived from velocity dispersion fixed by numerical simulations.

People wanting to estimate the mass of one or two clusters have to measure galaxy counts brighter than  $M_V = -20$  mag within the  $r_{200}$  radius estimated from equation (18) plus a similar measurement in an area devoid of cluster galaxies to account for background galaxies, list these values with our measurements and run the JAGS code listed in Appendix B. Those in a hurry and accepting a reduced quality of the mass estimation and of its uncertainty may simply insert the measured  $n_{200}$  in equation (19) and take a  $\pm 0.29$  dex mass error.

In Appendix A we present an individual comparison with the literature addressing the richness–mass scaling. Here we emphasize that our measurement of the performances of mass proxies conceptually differs from some other published works. (a) We quote the posterior predictive uncertainty and not the scatter. The former accounts for the uncertainty in the richness–mass scaling, while the latter does not. Since the scaling between mass and richness is not known perfectly, we prefer posterior predictive uncertainty to the

scatter. (b) Our own measurement of the scatter is not biased low, whereas literature values are sometimes biased low as a result of the way the best-fitting model is found, minimizing the scatter. The best-fitting relation is preferred (by other authors) to the true relation if this leads to a lower scatter. The effect is intuitively obvious (and quantitatively important) for small samples. We prefer, instead, not to be optimistic. (c) Some works (e.g. Lopes et al. 2009) evaluate the performances of a mass proxy assuming that mass-linked quantities such as  $r_{200}$  are known while they are unknown for clusters with unknown masses. This logical inconsistency has an important impact on the final result. Had we followed Lopes et al. (2009), we should have concluded that richness returns masses with a 0.19 dex precision, instead of with a 0.27 dex precision, almost a 50 per cent underestimate. (d) Some works, instead, forget important items, such as Malmquist bias. As detailed in Appendix A, where individual works are considered, generally speaking, authors tend to be more optimistic about the quality of the richness–mass calibration and the proxy performances than their data allow.

As mentioned, in order to use richness for cosmological studies, we need to check that our results hold for an optically selected cluster and, if a large redshift range is considered, we need to measure the evolution of the scaling, similarly to what is necessary for calibrating every other mass proxy. The first issue will be attacked by our (running) X-ray observations of an optically selected cluster sample, the second one by a lensing analysis of an intermediate redshift ( $0.3 < z < 0.8$ ) cluster sample. From this perspective, in this paper we also calibrated richness against cluster velocity dispersion, which are easier to measure than caustic masses. Evolution of red galaxies is now well understood (Kodama et al. 1998; Stanford, Eisenhardt & Dickinson 1998; De Propriis et al. 1999; Andreon 2006; Andreon et al. 2008b), quite differently from another widely used mass tracer, the X-ray emission from the intra-cluster medium. For the latter, one is forced to assume self-similar evolution for lack of better knowledge (e.g. Vikhlinin et al. 2009) even if available X-ray observations argue against this scenario (e.g. Markevitch 1998; Pratt et al. 2008).

## ACKNOWLEDGMENTS

We thank Vincent Eke and the anonymous referee for their useful comments that prompted us to insert Sections 3, 6.5 and 8. We also thank D. Johnston, A. Moretti, R. Trotta, L. Aguillar and E. Meyer for useful suggestions. For the standard SDSS acknowledgement, see, <http://www.sdss.org/dr6/coverage/credits.html>

## REFERENCES

Abell G. O., 1958, *ApJS*, 3, 211  
 Abell G. O., Corwin H. G., Jr, Olowin R. P., 1989, *ApJS*, 70, 1  
 Adelman-McCarthy J. K. et al. (SDSS Collaboration), 2008, *ApJS*, 175, 297  
 Akritas M. G., Bershadsky M. A., 1996, *ApJ*, 470, 706  
 Albrecht A. et al., 2006, Report of the Dark Energy Task Force (astro-ph/0609591)  
 Andreon S., 2006, *MNRAS*, 369, 969  
 Andreon S., 2008, *MNRAS*, 386, 1045  
 Andreon S., 2009, in *Bayesian Methods for cosmology*, Cambridge Univ. Press, Cambridge<sup>7</sup>

Andreon S., Willis J., Quintana H., Valtchanov I., Pierre M., Pacaud F., 2004, *MNRAS*, 353, 353  
 Andreon S., Punzi G., Grado A., 2005, *MNRAS*, 360, 727  
 Andreon S., Quintana H., Tajer M., Galaz G., Surdej J., 2006a, *MNRAS*, 365, 915  
 Andreon S., Cuillandre J.-C., Puddu E., Mellier Y., 2006b, *MNRAS*, 372, 60  
 Andreon S., De Propriis R., Puddu E., Giordano L., Quintana H., 2008a, *MNRAS*, 383, 102  
 Andreon S., Puddu E., de Propriis R., Cuillandre J.-C., 2008b, *MNRAS*, 385, 979  
 Bayes T., 1764, *Essay Towards Solving a Problem in the Doctrine of Chances*, Philos. Trans. R. Soc. Lond.  
 Becker M. R. et al., 2007, *ApJ*, 669, 905  
 Bergé J. et al., 2008, *MNRAS*, 385, 695  
 Biviano A., Murante G., Borgani S., Diaferio A., Dolag K., Girardi M., 2006, *A&A*, 456, 23  
 Blindert K., 2006, PhD thesis  
 Böhringer H. et al., 2001, *A&A*, 369, 826  
 Borgani S., Guzzo L., 2001, *Nat*, 409, 39  
 Bruzual G., Charlot S., 2003, *MNRAS*, 344, 1000  
 Carlberg R. G. et al., 1997, *ApJ*, 485, L13  
 D’Agostini G., 2003, *Bayesian Reasoning in Data Analysis – A Critical Introduction*. World Scientific Press, Singapore  
 D’Agostini G., 2004, preprint (astro-ph/0403086)  
 Dellaportas P., Stephens D., 1995, *Biometrics*, 51, 1085  
 De Lucia G. et al., 2007, *MNRAS*, 374, 809  
 De Propriis R., Stanford S. A., Eisenhardt P. R., Dickinson M., Elston R., 1999, *AJ*, 118, 719  
 Diaferio A., 1999, *MNRAS*, 309, 610  
 Diaferio A., Geller M. J., 1997, *ApJ*, 481, 633  
 Eddington A., 1940, *MNRAS*, 100, 354  
 Evrard A. E. et al., 2008, *ApJ*, 672, 122  
 Finoguenov A. et al., 2007, *ApJS*, 172, 182  
 Gal R. R., Lemaux B. C., Lubin L. M., Kocevski D., Squires G. K., 2008, *ApJ*, 684, 933  
 Gelman A., Carlin J., Stern H., Rubin D., 2004, *Bayesian Data Analysis*. Chapman & Hall/CRC, Boca Raton, FL  
 Gladders M. D., Yee H. K. C., 2005, *ApJS*, 157, 1  
 Gladders M. D., Yee H. K. C., Majumdar S., Barrientos L. F., Hoekstra H., Hall P. B., Infante L., 2007, *ApJ*, 655, 128  
 Hansen S. M., McKay T. A., Wechsler R. H., Annis J., Sheldon E. S., Kimball A., 2005, *ApJ*, 633, 122  
 Jeffreys H., 1938, *MNRAS*, 98, 190  
 Johnston D. E. et al., 2007, preprint (arXiv:0709.1159)  
 Kelly B. C., 2007, *ApJ*, 665, 1489  
 Kodama T., Arimoto N., Barger A. J., Aragón-Salamanca A., 1998, *A&A*, 334, 99  
 Koester B. P. et al., 2007a, *ApJ*, 660, 239  
 Koester B. P. et al., 2007b, *ApJ*, 660, 221  
 Kravtsov A. V., Vikhlinin A., Nagai D., 2006, *ApJ*, 650, 128  
 Laplace P.-S., 1812, *Théorie Analytique des Probabilités*  
 Lin Y.-T., Mohr J. J., Stanford S. A., 2004, *ApJ*, 610, 745  
 Lopes P. A. A., de Carvalho R. R., Kohl-Moreira J. L., Jones C., 2009, *MNRAS*, 399, 220  
 MacKay D., 2003, *Information Theory, Inference and Learning Algorithms*. Cambridge Univ. Press, Cambridge  
 Majumdar S., Mohr J. J., 2004, *ApJ*, 613, 41  
 Mandelbaum R., Seljak U., 2007, *J. Cosmology Astropart. Phys.*, 6, 24  
 Mandelbaum R., Seljak U., Hirata C. M., 2008, *J. Cosmology Astropart. Phys.*, 8, 6  
 Markevitch M., 1998, *ApJ*, 504, 27  
 Maughan B., 2007, *ApJ*, 668, 772  
 Muchovej S. et al., 2007, *ApJ*, 663, 708  
 Muzzin A., Yee H. K. C., Hall P. B., Lin H., 2007, *ApJ*, 663, 150  
 Oemler A. J., 1974, *ApJ*, 194, 1  
 Pacaud F. et al., 2007, *MNRAS*, 382, 1289

<sup>7</sup> <http://www.brera.mi.astro.it/~andreon/MYPUB/statbook.pdf>

- Plummer M., 2008, JAGS Version 1.0.3 user manual<sup>8</sup>  
 Pratt G. W., Croston J. H., Arnaud M., Boehringer H., 2008, A&A, in press (arXiv:0809.3784)  
 Rasia E. et al., 2006, MNRAS, 369, 2013  
 Rines K., Diaferio A., 2006, AJ, 132, 1275  
 Rines K., Diaferio A., 2010, AJ, 139, 580  
 Rines K., Geller M. J., Kurtz M. J., Diaferio A., 2003, AJ, 126, 2152  
 Rozo E. et al., 2007, preprint (astro-ph/0703571)  
 Rozo E. et al., 2009, ApJ, 703, 601  
 Rozo E. et al., 2010, ApJ, 708, 645  
 Rykoff E. S. et al., 2008, ApJ, 675, 1106  
 Schuecker P., Böhringer H., Voges W., 2004, A&A, 420, 61  
 Scoville N. et al., 2007, ApJS, 172, 1  
 Sheldon E. S. et al., 2009, ApJ, 703, 2232  
 Spiegelhalter D., Thomas A., Best N., Gilks W., 1996, BUGS: Bayesian Inference Using Gibbs Sampling, Version 0.5<sup>9</sup>  
 Stanek R., Evrard A. E., Böhringer H., Schuecker P., Nord B., 2006, ApJ, 648, 956  
 Stanford S. A., Eisenhardt P. R., Dickinson M., 1998, ApJ, 492, 461  
 Trotta R., Bower R., 2006, Astron. Geophys., 47, 20  
 Vikhlinin A. et al., 2009, ApJ, 692, 1060  
 Wu H.-Y., Rozo E., Wechsler R. H., 2008, ApJ, 688, 729  
 Zwicky F., 1957, Morphological Astronomy. Springer-Verlag, Berlin

## APPENDIX A: COMPARISON WITH PREVIOUS WORKS

The comparison of our results with previous works uses a reduced model, because part of the data needed for our full analysis is unpublished. Generally speaking, previous works did not publish observed values of background and total counts, *obsbkg* and *obstot*, but just  $obsn200 = obstot - obsbkg/C$  and assumed the latter quantity (an observed value) to be equal to  $n200$  (the true value).

In the maxBCG work, such an identification leads to a significant bias, as discussed later. In the other works, such identification is safer, but authors systematically underestimate their uncertainties either assuming that the mass–richness scaling has no intrinsic scatter, or that the slope of the scaling is perfectly known, for example when the intrinsic scatter is derived.

Rines et al. (2003) compute  $N_{200}$  values for a sample of nine clusters with available caustic masses. Their scaling, derived by a least-squares fit, has *inverse* slope  $0.70 \pm 0.09$ . Our revised model now assumes that the observed richness is Gaussian distributed with mean  $n200$  and standard deviation  $obserrn200$  and an uniform prior on  $n200$ . In formulae, equations (5), (6), (12) and (13) are replaced by

$$obsn200_i \sim \mathcal{N}(n200_i, obserrn200_i^2), \quad (A1)$$

$$n200_i \sim \mathcal{U}(0, \infty). \quad (A2)$$

With our model, which allows an intrinsic scatter that their least-squares fit does not, we found (using their data kindly made available to us) a slope of  $1.23 \pm 0.25$ , in agreement with our determination using a larger sample. The slope error we found in their data is about twice as large as that we found in our data (our sample is six times bigger) and is larger than their quoted slope error, derived assuming no intrinsic scatter (and also no noisiness of mass errors). The 95 per cent confidence interval on the intrinsic scatter derived

with this small sample largely depends on the adopted prior, in contrast to what we find with our larger sample.

Muzzin et al. (2007) measure  $N500$  for a sample of 15 clusters (one of which is discarded a posteriori) with dynamical masses (i.e. coming from a velocity dispersion measurement). They use masses and richnesses within  $r_{500}$ ,  $M500$  and find a slope of  $1.40 \pm 0.22$  with mass. Their slope is at 1.6 combined  $\sigma$  from the slope we derive for our sample. However, their uncertainty on the found slope assumes that no intrinsic scatter is there and once one is allowed, their errors escalate and the difference between the two slopes, in terms of combined  $\sigma$ , decreases.

For 25 clusters in the Red Cluster Sequence Survey (RCS, Gladders & Yee 2005), Blindert (2006) computes the scaling between the RCS richness,  $B_{gcr}$ , and velocity dispersion. Their richness only uses red galaxies, as does ours. We note, however, that their velocity dispersions  $s$  are derived from a small number of velocities ( $<25$  for about half the sample, versus our average of 208 velocities per cluster) and thus have low reliability (Gal et al. 2008; Andreon et al. 2008a; Andreon 2009). They found a slope of  $0.75 \pm 0.57$ , which is entirely consistent with our, better determined, slope of  $0.30 \pm 0.04$ , given Blindert (2006)’s large errors.

Johnston et al. (2007) stack maxBCG (Koester et al. 2007a) clusters, derive masses from lensing and measure the scaling between richness and the derived masses. For our present purposes, it is probably of little relevance that their *obsn200*, counting by definition galaxies within  $r_{200}$ , counts instead galaxies within  $2r_{200}$ . They obtain a slope of  $1.28 \pm 0.04$ , much more precise than our slope, which has an error of 0.15, at least at first sight. Johnston et al.’s (2007) statistical analysis is quite complex. Let us consider just a single aspect, Johnston et al. (2007) did not account for the difference between the observed value, *obsn200* and the true value  $n200$ .<sup>10</sup> Errors introduce a scatter between  $n200$  and *obsn200* and, because of the large abundance of clusters of low richness, the scatter brings many more low-richness clusters up than high-richness clusters down. This implies that a given observed richness, *obsn200*, many objects have indeed a  $n200 < obsn200$ . This selection effect, usually called Malmquist or Eddington bias, is especially large for the maxBCG clusters, whose observed richness is as low as 3. Let us compute the Malmquist or Eddington correction; in mathematical terms,  $p(n200|obsn200) \propto p(obsn200|n200) p(n200)$  (Bayes theorem). The cluster number counts in Johnston et al. (2007) paper have a logarithmic slope of about  $-3$  ( $=\partial \log n / \partial \log n200$ ). This is the adopted logarithmic slope of the prior  $p(n200)$ . The likelihood,  $p(obsn200|n200)$ , is Poisson. Performing the algebra, it turns out that on average  $n200 \sim obsn200 - 2$ , as qualitatively expected. If we now refit the Johnston et al. (2007) richness–mass data using Malmquist corrected values (i.e. using  $obsn200 - 2$ ), we got a slope of  $\approx 1.0$ . This is about  $7\sigma$  away from the quoted value, if we trust the slope error as published by Johnston et al. (2007), this shows that their slope is not robust and their slope error is largely underestimated. As stressed by Jeffreys (1938) and Eddington (1940), our correction above has to be taken as an indication, by no means as a replacement of the correct analysis. It has been presented only to give a glimpse of its size. Our finding that the mass–richness calibration by Johnston et al. (2007) is more uncertain than claimed is also supported by the result of a very similar but independent lensing analysis by Mandelbaum, Seljak & Hirata (2008).

<sup>8</sup>[http://calvin.iarc.fr/~martyn/software/jags/jags\\_user\\_manual.pdf](http://calvin.iarc.fr/~martyn/software/jags/jags_user_manual.pdf)

<sup>9</sup><http://www.mrc-bsu.cam.ac.uk/bugs/documentation/Download/manual05.pdf>

<sup>10</sup> This difference is instead considered when the distribution of *obsn200* is used to constrain cosmological parameters in Rozo et al. (2010).

Lin, Mohr & Stanford (2004) compute the richness–mass scaling for a large cluster sample and found a slope about  $1\sigma$  away from our one, but with very small errors. However, their masses are derived from X-ray temperatures, in turn assumed to be perfectly known (even in presence of large temperature errors), although they have been derived in heterogeneous ways (e.g. from measurements performed in heterogeneous selected apertures, with or without flagging the cool core, etc.) from heterogeneous data/telescopes. Furthermore, temperature–mass scaling is assumed to be perfectly known, without any scatter and valid for clusters not in hydrostatic equilibrium, none of which is true. Similarly, the radius within which richness is computed is estimated from cluster temperature, assuming no scatter between temperature and mass. Therefore, the small errors quoted by Lin et al. (2004) are found in an analysis where masses and radii are assumed to be perfectly known, in spite of their significant noisiness and, possibly, bias.

## APPENDIX B: MODEL LISTING

In this section we give the listing of the full model.

For the stochastic computation and for building the statistical model, we use Just Another Gibbs Sampler (JAGS,<sup>11</sup> Plummer 2008). Equations (5)–(15) find an almost literal translation in JAGS, Poisson, Normal and Uniform distributions become `dpois`, `dnorm` and `dunif`, respectively. JAGS, following BUGS (Spiegelhalter et al. 1996), uses precisions,  $prec = 1/\sigma^2$ , in place of variances  $\sigma^2$ . Furthermore, it uses neperian logarithms, instead of decimal ones. Equation (6) has been rewritten using the property that the  $\chi^2$  is a particular form of the Gamma distribution. Equation (7) is split in two JAGS lines for a better reading. The arrow symbol reads ‘take the value of’. `obsvarlgM200` is the square of `obserrlgM200`.

<sup>11</sup> <http://calvin.iarc.fr/~martyn/software/jags/>

```
data
{
  nu <- -6
}
model
{
  for (i in 1:length(obstot)) {
    obsbkg[i] ~ dpois(nbkg[i])
    obstot[i] ~ dpois(nbkg[i]/C[i]+n200[i])
    n200[i] ~ dunif(0, 3000)
    nbkg[i] ~ dunif(0, 3000)

    precy[i] ~ dgamma(1.0E-5, 1.0E-5)
    obslgM200[i] ~ dnorm(lgM200[i], precy[i])
    obsvarlgM200[i] ~ dgamma(0.5*nu, 0.5*nu*precy[i])

    z[i] <- alpha+14.5+beta*(log(n200[i])/2.30258-1.5)
    lgM200[i] ~ dnorm(z[i], prec.intrscat)
  }
  intrscat <- -1/sqrt(prec.intrscat)
  prec.intrscat ~ dgamma(1.0E-5, 1.0E-5)
  alpha ~ dnorm(0.0, 1.0E-4)
  beta ~ dt(0, 1, 1)
}
```

In order to evaluate equation (4), i.e. to determine the uncertainty of the predicted mass, we simply need to add to the data file the list of clusters for which we want predictions. In this paper we used the same sample, as mentioned in Section 7, which is, as a result, listed twice in the data file, the second time with ‘NA’ (‘not available’) values of mass indicating the program with which they should be estimated.

This paper has been typeset from a  $\text{\LaTeX}$  file prepared by the author.